

## 2. DIFFRACTION GEOMETRY AND ITS PRACTICAL REALIZATION

The method can also be used with a receiving slit or position-sensitive detectors (Lehmann *et al.*, 1987; Shishiguchi, Minato & Hashizume, 1986). The latter can be a short straight detector, which can be scanned to increase the data-collection speed (Göbel, 1982), or a longer curved detector.

## 2.3.2.3. Grazing-incidence diffraction

In conventional focusing geometry, the specimen and detector are coupled in  $\theta$ - $2\theta$  relation at all  $2\theta$ 's to avoid defocusing and profile broadening. In Seemann-Bohlin geometry, changing the specimen position necessitates realigning the diffractometer and very small incidence angles are inaccessible. In parallel-beam geometry, the specimen and detector positions can be uncoupled without loss of resolution. This freedom makes possible the use of different geometries for new applications. The specimen can be set at any angle from grazing incidence to slightly less than  $2\theta$ , and the detector scanned. Because the incident and exit angles are unequal, the relative intensities may differ by small amounts from those of the  $\theta$ - $2\theta$  scan due to specimen absorption. The reflections occur from differently oriented crystallites whose planes are inclined (rather than parallel) to the specimen surface so that particle statistics becomes an important factor. The method is thus similar to Seemann-Bohlin but without focusing.

The method can be used for depth-profiling analysis of polycrystalline thin films using grazing-incidence diffraction (GID) (Lim, Parrish, Ortiz, Bellotto & Hart, 1987). If the angle of incidence  $\theta_i$  is less than the critical angle of total reflection  $\theta_c$ , diffraction occurs only from the top 35 to 60 Å of the film. Comparison of the GID pattern with a conventional  $\theta$ - $2\theta$  pattern in which the penetration is much greater gives structural information for phase identification as a function of film depth. The intrinsic profile shapes are the same in the two patterns and broadening may indicate smaller particle sizes. However, if the film is epitaxial or highly oriented, it may not be possible to obtain a GID pattern.

For  $\theta_i < \theta_c$ , the penetration depth  $t'$  is (Vineyard, 1982)

$$t' \simeq \lambda / [2\pi(\theta_c^2 - \theta_i^2)^{1/2}] \quad (2.3.2.1)$$

and, for  $\theta_i > \theta_c$ ,

$$t' \simeq 2\theta_i / \mu, \quad (2.3.2.2)$$

where  $\mu$  is the linear absorption coefficient. The thinnest top layer of the film that can be sampled is determined by the film density, which may be less than the bulk value. As  $\theta_i$  approaches  $\theta_c$ , the penetration depth increases rapidly and fine control becomes more difficult. Fig. 2.3.2.7 shows this relation and the advantage of using longer wavelengths for a wider range of penetration control. For example, for a film with  $\mu = 200 \text{ cm}^{-1}$ ,  $\lambda = 1.75 \text{ Å}$ , and  $\theta_i = 0.1^\circ$ , only the top 45 Å contribute, and increasing  $\theta_i$  to  $0.35^\circ$  increases the depth to 130 Å. The patterns have much lower intensity than a  $\theta$ - $2\theta$  scan because of the smaller diffracting volume.

Fig. 2.3.2.8 shows patterns of a 5000 Å polycrystalline film of iron oxide deposited on a glass substrate and recorded with (a)  $\theta$ - $2\theta$  scanning and (b)  $0.25^\circ$  GID. The film has preferred orientation as shown by the numbers above the peaks in (a), which are the relative intensities of a random powder sample. The relative intensities are different because in (a) they come from planes oriented parallel to the surface and in (b) the planes are inclined. The glass scattering that is prominent in (a) is absent in (b) because the beam does not penetrate to the substrate.

## 2.3.2.4. High-resolution energy-dispersive diffraction

By step scanning the channel monochromator instead of the specimen, a different wavelength reaches the specimen at each step and the pattern is a plot of intensity versus wavelength or energy (Parrish & Hart, 1985, 1987). The X-ray optics can be the same as described in Subsection 2.3.2.1 and determines the resolution. A scintillation counter with conventional electronic circuits can be used. As in the conventional white-beam energy-

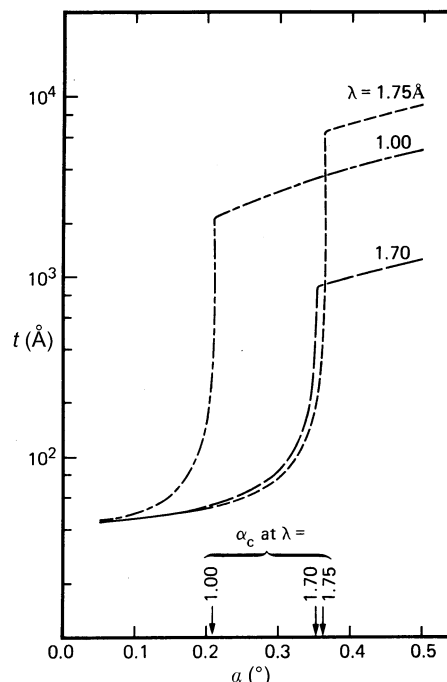


Fig. 2.3.2.7. Penetration depth  $t'$  as a function of grazing-incidence angle  $\alpha$  for  $\gamma\text{-Fe}_2\text{O}_3$  thin film. The critical angle of total reflection  $\alpha_c$  is shown by the vertical arrows for different wavelengths.

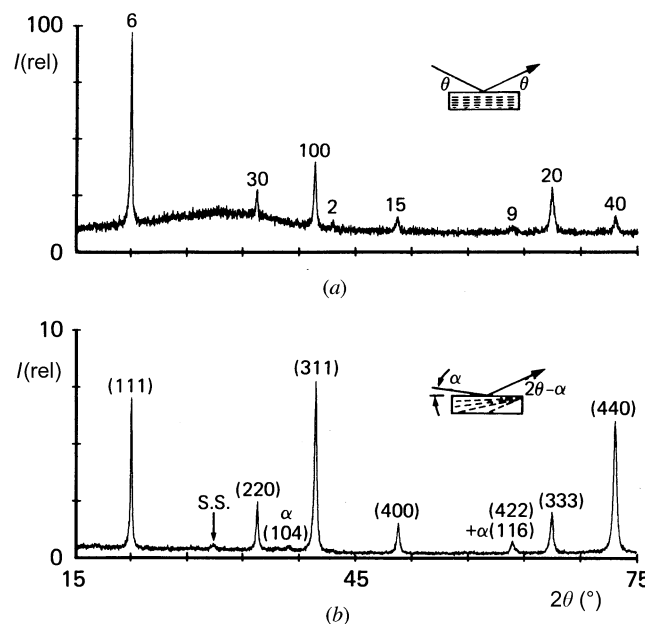


Fig. 2.3.2.8. Synchrotron diffraction patterns of annealed 5000 Å iron oxide film,  $\lambda = 1.75 \text{ Å}$ , (a)  $\theta$ - $2\theta$  scan; relative intensities of random powder sample shown above each reflection. (b) Grazing incidence pattern of same film with  $\alpha = 0.25^\circ$  showing only reflections from top 60 Å of film, superstructure peak S.S. and  $\alpha\text{-Fe}_2\text{O}_3$  peaks not seen in (a). Absolute intensity is an order of magnitude lower than (a).